Cost-effective, low density, carbon soot doped resorcinol formaldehyde composite for ablative applications

Yutika Badhe,[a] Balasubramanian K*[a] and Rohit Gupta[b]

Successful *in situ* polymerization of highly ablation-resistant composites of resorcinol formaldehyde (RF) modified with carbon soot (CS) was carried out for the first time. The composites exhibited a comparatively high char yield, up to 59.7% at 800 °C, and while undergoing ablation by an oxyacetylene flame displayed exceptionally low linear and mass ablation rates of 0.019 mm s^{-1} and 0.053 g s^{-1}, respectively. Microstructure analysis of a surface ablated for 60 s revealed a uniform pattern of closely knit carbon nanobead-like structure which ensured enhanced ablation resistance. The formation of turbostratic carbon guaranteed a significantly improved thermal insulation property of the ablative composite at a higher temperature. An XRD graph showed peaks at 24° and 44°, corresponding to carbon nanobeads and insulating turbostratic carbon. The ability of RF to replace conventional phenol formaldehyde (PF) resin was confirmed. A CS/RF ablative composite during ablation also displayed reduced erosive losses and hence can be potentially used as a backbone material of a thermal protection system required for ablative applications.

Introduction

One of the most interesting complications of a space program is the safe re-entry of blunt-nosed rocket vehicles *via* effective heat transfer phenomena. Improper measures and insufficient precautions may lead to fatal accidents, due to hostile aerothermal conditions, as in the case of the space shuttle Columbia.[1] In this regard, ablative materials and thermal protection systems (TPS) have been significantly used for insulation applications,[2] ranging from payloads and ground equipment to main propulsion systems. Ablation is a series of endothermic erosive processes involving complex pyrolytic and charring reactions, leading to high heat fluxes dissipated by insulating materials protecting the rocket body during atmospheric re-entry. Most of the surface radiation, phase transitions and chemical reactions are responsible for counteracting the convective heat that reaches the vehicle. Moreover, part of the incoming convective heat flux is blocked by the outgoing flow of hot gases that result from the degradative processes.

Polymer matrix composites (PMCs) are becoming favoured materials[3] for engineering lightweight and strong parts for TPS used for ICBM nozzles, rocket exhausts, space vehicles *etc.* However, among the various types of such matrices used, the char layer formed upon ablation is relatively weak[4] as it can be mechanically eroded by frictional forces brought about by the rocket combustion products or the aerodynamic drag of atmospheric gases. Phenol formaldehyde (PF) is a preferred thermosetting resin because of its high ablation resistance and ability to form char efficiently during pyrolysis.[5] Despite its erosion resistance and capacity for char retention, phenol formaldehyde (PF) has been modified with atoms having high bond energies (boron, molybdenum, titanium and phosphorus),[6–11] nanosized inorganic cage structures such as OP-POSS (octaphenol polyhedral oligomeric silsesquioxane),[12] thermally resistant hyperbranched polyborate (HBPB),[13] silicone resin-based anti-ablation coatings,[14] nanoclay additives in phenolic resin[15,16] or changes in the weave patterns of carbon fabric or silica fibre[17,18] to improve their ablation resistance. However, there is always a need to have a strengthened char layer for improved ablation resistance in order to formulate a relatively thin ablative system to reduce the overall weight of the TPS. In this work, resorcinol was chosen over phenol owing to its unique molecular structure, which provides three relatively more reactive sites for formaldehyde to react with. Badhe *et al.* proposed the use of resorcinol instead of phenol to synthesize a resol-type thermoset which proved to have lower density and higher thermal stability than PF.[19] Resorcinol-formaldehyde (RF) is recognised for its dry-bonding and cold-setting adhesive properties, which are put to use primarily in manufacturing structural finger joints and timber structures for providing exceptional strength and weather-resistant bonding. The presence of two hydroxyl groups at *meta* positions in resorcinol, as compared to one in phenol, gives rise to additional crosslinking

[a]*DIAT(DU), Ministry of Defence, Government of India, Materials Engineering, Pune, Maharashtra, India. E-mail: meetkbs@gmail.com*

[b]*Indian Institute of Technology – Banaras Hindu University, Department of Ceramic Engineering, Varanasi, Uttar Pradesh, India*

due to highly reactive sites and faster curing.[20] Moreover, due to an increase in crosslinking, the resin structure becomes more stable and its thermal conductivity is found to be in the range 0.30–0.58 W m^{-1} K^{-1}, which is considerably reduced, compared to the reported value of 0.59 W m^{-1} K^{-1} for PF resins.[21,22] Resorcinol exhibits a unique molecular structure, due to the location of the two hydroxyl groups in the molecule. It gives rise to three reactive sites or positions in the resorcinol molecule for formaldehyde to react with. All three reactive positions of resorcinol are doubly activated by the two hydroxyl groups.[20,23] Thus resorcinol, having two –OH groups in its structure, provides faster reaction rates and has the ability to cure at room temperature, consequently being energy-efficient. The reactivity of resorcinol is about twelve times that of phenol with formaldehyde under similar conditions.[20,24–26] Conventional phenol formaldehyde, on the other hand, forms bubbles and blisters on its surface if cured without pressures of 15–30 MPa.[5,27]

However, to constantly surpass conventional resins in terms of thermal and physical properties like low density and lower ablation rates, taking into account the high costs involved, continuous progress takes place in synthesizing suitable replacements. In one such attempt, efforts were made to use amorphous carbon soot as a filler, which exhibits a vast range of applications, owing to its different bond hybridisations.[28] The various precursors used for the synthesis of amorphous carbon or carbon nanobeads are methane, ethylene, acetylene, *etc.*[29,30] Research literature focusing on the synthesis of carbon nanostructures, such as DLC, carbon nanobeads, CNTs, graphene, and fullerene *via* thermal decomposition of an eco-friendly, cheap and renewable hydrocarbon, camphor ($C_{10}H_{16}O$), using CVD[31] are also reported. Camphor is a fragrant hydrocarbon consisting of both sp^3 and sp^2-hybridised carbons.[32] Upon combustion, the three methyl groups of camphor become detached from its skeleton, yielding highly reactive ring structures,[33] which are responsible for the formation of three-dimensional spherically shaped carbon nanomaterials.[34,35]

The present study, therefore, focuses on the synthesis of a novel ablative composite of resorcinol formaldehyde (RF) reinforced with carbon soot (CS) particles and investigation of its ablative applications for critical purposes associated with re-entry probes, missile nozzles, wing flanges and ballistic aeroshells in space shuttle programs. RF resins in their pristine form prove to be better ablative agents than conventional phenol formaldehyde, as shown by Badhe *et al.*[19,36] Furthermore, efforts have been made towards employing an extremely efficient and facile soot-based approach for the preparation of luminescent CNPs. This provides a simple and effective route for the extraction of photoluminescent carbon soot particles from the combustion of camphor, incorporating them in various concentrations with RF and studying their effects and thermal resistance properties.

The present work aims at establishing a comparative study between conventional phenolic resin and resorcinol formaldehyde, synthesized *via* an *in situ* polymerization technique with camphor soot nanoparticles. The work has been extended to study the effects of the incorporation of CS nanoparticles on the product's insulating nature and thermal degradation process.

Changes in the microstructure and surface topography were also studied with respect to hydrophobicity and the formation of a closely knit nanobead structure after ablation.

Sahoo *et al.* have been successful in carrying out the synthesis of catalyst-free photoluminescent carbon nanoparticles derived from the combustion of camphor in a single-step flame process, exhibiting a diamond-like carbon nanostructure.[35] These nanosized camphor soot particles were derived *via* a cost-effective, non-energy-intensive process from the combustion of camphor, in the absence of a precursor, in a perforated polycarbonate chamber which aids lean combustion with an appreciable yield. HR-TEM imaging was used to display the formation of carbon nanoparticles, along with their size and the interlinking of the carbon nanoparticles. Fig. 1 shows an HR-TEM image of camphor soot particles of an average size of 30–70 nm aggregated together in a necklace-like interconnected pattern. An extensive study on the formation and analysis of these camphor soot nanoparticles can be found in the study conducted by Sahoo *et al.*[35] The applications of these novel CNPs have been extensively explored, ranging from super-hydrophobicity and oil absorption from spills to uranium uptake for water treatment.[35–39] To further explore the multiple applications of the synthesized CNPs, a study of ablative composites was performed, by virtue of the excellent thermal stability of carbonaceous materials, and the system displayed better performance than most of the studies reported to date.

Despite having studied the effects of other carbon fillers with phenolic resins, researchers have not explored resorcinol formaldehyde and carbon fillers for ablative composites. The following table (Table 1) contrasts the performance of previous systems with carbonaceous fillers and the present system.

Experimental

Materials

Resorcinol (crystalline, 98% purity) and formalin solution (37 wt% formaldehyde in water containing 10–15% methanol as stabilizer) were procured from Sigma Aldrich Chemicals Pvt Ltd, USA. Camphor tablets of size 7×5 mm ($C_{10}H_{16}O$, 96%, Sigma Aldrich Chemicals Pvt Ltd, USA) were used as a source for carbon soot particles without any further purification. 20 wt%
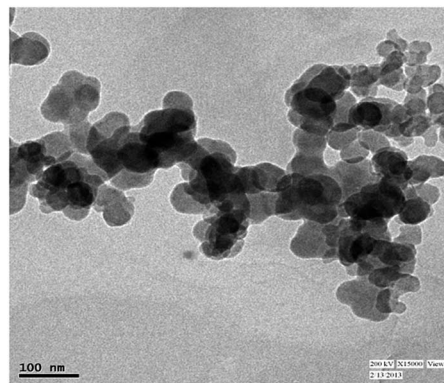

Fig. 1 HR-TEM image of camphor soot particles.

Table 1 Comparison between the existing literature on carbon composites and the present system[5,15,40–45]

Sr. no.	Composite system in the literature	Characteristic of the literature	Characteristic of the present system
1.	Vapour-grown carbon fibre filled in phenolic resin[15]	30–50 wt% filler	1–10 wt%
		Test carried out for 20 s at ~1650 °C	Test carried out for 60 s at ~3000 °C
		LAR = 1.689 μm s^{-1}	LAR = 0.023 mm s^{-1}
		Expensive	Cost-effective
2.	Carbon black + MWNT/phenolic resin[40]	50 wt% filler	10 wt% filler
		Back-face temperature after 300 s was 100 °C	Back-face temperature after 300 s was ~80 °C
3.	Phenolic impregnated 3-D fine-woven pierced carbon fabric ablator (PICA)[41]	Expensive	Cost-effective
		MAR = 0.061 g s^{-1}	MAR = 0.056 g s^{-1}
		LAR = 0.036 mm s^{-1}	LAR = 0.023 mm s^{-1}
4.	C/C Ph composite[42]	LAR = 0.023 mm s^{-1}	LAR = 0.023 mm s^{-1}
5.	C/C composite[5]	Test carried out at ~2000 °C	Test carried out at ~3000 °C
		LAR = 0.17 μm s^{-1}	LAR = 0.023 mm s^{-1}
6.	Functionally grafted carbon fiber + phenolic[44]	LAR = 0.103 mm s^{-1}	LAR = 0.023 mm s^{-1}
7.	3 dimensional C fibre/SiC[43]	Test carried out at ~1900 °C for 55 s	Test carried out at ~3000 °C for 60 s
		LAR = 0.064 mm s^{-1}	LAR = 0.023 mm s^{-1}
		MAR = 0.027 g s^{-1}	MAR = 0.056 g s^{-1}
8.	3 dimensional C fibre/ZrC[45]	Test carried out at ~2028 °C for 60 s	Test carried out at ~3000 °C for 60 s
		LAR = −0.002 mm s^{-1}	LAR = 0.023 mm s^{-1}
		MAR = 0.012 g s^{-1}	MAR = 0.056 g s^{-1}

NaOH solution was prepared using sodium hydroxide pellets manufactured and supplied by Merck (India) and deionized water. Deionized water was used for all 75 of the experiments and was obtained from a Millipore Milli-Q system.

Methods

An in-house setup for the combustion of camphor tablets was developed by Sahoo *et al.*[35] in order to examine the controlled combustion process and its repeatability. The same method was used in this experiment, by placing a camphor tablet of size 7 × 5 mm ($L \times D$) in a silica crucible (25 mL) which was enclosed inside a polycarbonate (PC) chamber with holes of 5 mm diameter (Fig. 2). The PC setup was then placed inside a Haier laminar flow chamber (Model: HR30:IIA2) during the soot collection process. A controlled laminar flow was ensured at a constant down-flow velocity of 0.30 m s^{-1} through the holes of the chamber. As a result, recirculating air was constantly made available for efficient lean combustion, aided by the oxygen atom in camphor ($C_{10}H_{16}O$), and consequently providing a higher yield of soot. It was observed that within the stipulated time duration, the emitted soot particles were collected in a layered pattern over the glass substrate. The collected camphor soot particles were stored in glass bottles without any post-treatment.

A typical formulation of the composite involved different wt% of CS particles (0, 1, 2, 3, 5, 10) added slowly to a continuously stirred mixture of resorcinol and formaldehyde, which was blended in the molar ratio $F/R = 2$. To this mixture, 0.5 mL of 10 wt% NaOH solution was added dropwise giving a complex 3-dimensional crosslinked polymer chain network. As resorcinol is highly reactive, the temperature of the mixture was strictly restricted between 50 and 60 °C to avoid immediate setting of the resin. All samples were kept in a 20 × 40 mm ($L \times D$) cylindrical mould and were cured for 4 hours at 60 °C. The synthesis of PF was carried out in a similar fashion for comparing the results with our system, except the reaction was carried out for another 1.5 h and the reaction temperature was maintained at around 100 °C.

Characterization

Ablative characteristics like the linear ablation rate (LAR) and mass ablation rate (MAR) were assessed by exposing the samples to a cheap, yet effective, oxyacetylene flame for 60 s. Practical artificial ablative test conditions were imitated using an oxyacetylene flame and a test specimen of 40 × 20 mm ($D \times T$ 95 dimensions) according to ASTM E285.

The inner diameter of the oxyacetylene torch tip was 2 mm and 10 mm distance was maintained between the torch tip and the sample. The flow rates of oxygen and acetylene were 1.960
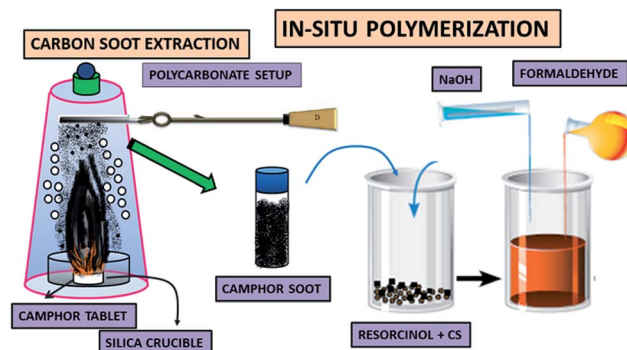

Fig. 2 Extraction of carbon nanoparticles from camphor and *in situ* polymerization of RF/CS composites.

and 0.696 L s^{-1}, respectively, which generated a flame temperature of around 3000 °C during the test. After ablation, the weight loss and dimensional changes of the specimens were evaluated to calculate the LAR and MAR using the following equations:[46]

$$LAR = dl/dt$$

$$MAR = dm/dt$$

where dl and dm represent the change in length and mass loss with respect to time dt.

Thermogravimetric analysis (TGA) was performed to investigate the thermal stability of OP-POSS/RF nanocomposites using a Perkin-Elmer Pyris1 TGA (USA) instrument operated at a heating rate of 10 °C min^{-1} from 25 °C to 800 °C in a nitrogen atmosphere at a flow rate of 100 mL min^{-1}. Furthermore, to comprehend the effect of the addition of CS to polymer resin on its surface barrier properties, contact angle measurement was conducted using a Kruss DSA100 (Germany) goniometer interfaced with image-capture software. An 8 μL deionised water drop at 25 °C was delivered from a microsyringe onto the polymer surface to form a sessile drop to determine the contact angle. Signatures obtained via XRD (Bruker AXS D8 Advance diffractometer, USA) and FESEM images (Carl Zeiss AG, Germany) were obtained to facilitate understanding of the composition and microstructure alteration that occurred due to ablation.

Results and discussion

Physical properties

The *in situ* polymerization involved pre-treatment by ultrasonication of CS particles for 10 min, followed by strong mechanical stirring of the reaction mixture. Composites without ultrasonication gave rise to agglomerated particles in the matrix, as shown by Fig. 3(a). Ultrasonication pre-treatment was performed to ensure homogeneous dispersion and deagglomeration of the carbon nanoparticles, due to propagation of sound waves resulting in alternating compressions and rarefactions in the liquid media. Individual particles of carbon soot are held together by attractive forces like van der Waals forces and the surface tension of the liquid, overcoming which is mandatory for uniform dispersion of the nanoparticles. The propagation of ultrasound in a medium causes oscillation of particles about their mean position and thus a change in the average distance between them arises.[47] As the negative pressure of the wave propagating in the medium exceeds a threshold value, the distance between the liquid and the molecules exceeds the minimum molecular distance which is required to keep the liquid intact, resulting in the formation of voids known as cavitation bubbles.[48–51] Ultrasonic cavitation generates high shear forces that break particle agglomerates into single dispersed particles. Hence, ultrasonication was used as a pre-treatment for the reaction mixture to ensure dispersed carbon nanoparticles in the matrix, which would get trapped in the three-dimensional matrix of resorcinol formaldehyde,
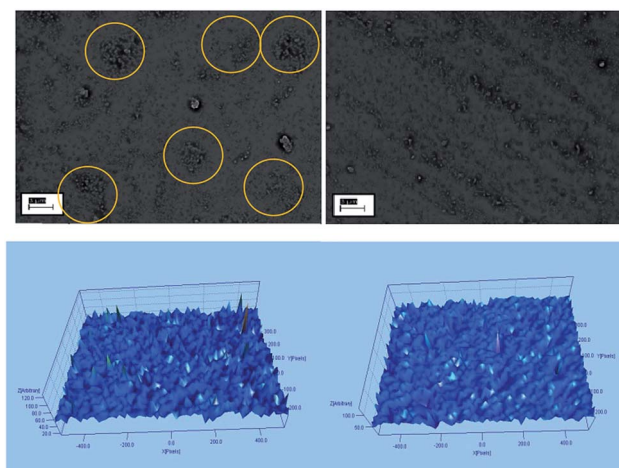

Fig. 3 Morphology of (a) the surface of RF + CS without ultrasonication treatment with visible agglomerates, (b) the surface of RF + CS composite after ultrasonication. 3-dimensional representation of (c) non-ultrasonicated RF/CS and (d) ultrasonicated RF/CS.

uniformly resist heat flux, resulting in an ordered segregated molecular-level dispersion. The most efficient place inside the ultrasonication bath was determined using a simple experiment described by Santos *et al.*, 'the aluminium foil test'.[48,51] A series of aluminium foil pieces of the same size were placed inside the bath and ultrasonicated. Cavitation in the ultrasonication bath causes perforations in the aluminium foil.[51] The sheet with the maximum number of perforations accurately identified the region of maximum intensity. The intensity profile displayed a profile similar to a Gaussian curve. The maximum perforations were found in the centre of the bath, while there were fewer perforations towards the bottom and top of the bath. Hence, the system was placed in the centre of the bath for maximum intensity.[51] Along with its position, the shape of the vessel is critical, as vessels with a flat base reflect a minimum amount of energy, while with round bases the ultrasonic waves impinge at an angle, causing most of the energy to reflect back.[50–52] Ultrasonic pre-treatment in a flat-based beaker kept in the centre of the bath gave a distribution in the matrix as shown by Fig. 3(b). Fig. 3(c) and (d) compare the roughness of the surfaces of the samples on a 3-dimensional scale. The non-uniformity in the surface of the composite without ultrasonication gave a roughness of 75.41 nm, in contrast with the 70.82 nm found for the composites which were ultrasonicated.

CS particles have a high surface area, which allowed them to cover the entire surface of the polymer matrix even at 1 wt% loading.[35] They have an extremely low bulk density, which was found to be as low as 0.043 g cm^{-3}. The density of RF, 1.26 g cm^{-3}, was lower than that of PF, 1.39 g cm^{-3}, and it further decreased to 1.19 g cm^{-3} as the concentration of CS in the polymer resin increased to 10 wt%, as indicated in Table 2.[36] The bulk volume of the polymer composite underwent an increase, due to the introduction of low-density camphor soot nanoparticles in between the chains of the amorphous polymeric resin structure, leading to a reduction in density. Furthermore, the higher homogeneity of the filler ensures

Table 2 Ablation rates and char density variations with weight% of camphor soot

Sample name	LAR (mm s^{-1})	MAR (g s^{-1})	Density (g cm^{-3})	%Char yield
Pure PF	0.054	0.087	1.39	40.5
Pure RF	0.050	0.079	1.26	45.8
1% CS + RF	0.041	0.069	1.25	56.9
2% CS + RF	0.031	0.063	1.24	57.1
3% CS + RF	0.024	0.057	1.23	58.8
5% CS + RF	0.019	0.053	1.21	59.7
10% CS + RF	0.023	0.056	1.19	59.6

nanocomposites with improved ablation behaviour and was anticipated to provide enhanced ablation resistance and thermal stability.[19,36]

Ablation rates

An oxyacetylene flame test, which recreates practical re-entry conditions involving shear and erosive forces at a temperature around 3000 °C,[41,53] was performed on all samples as per ASTM E-285. Fig. 4 shows photographs of the stages of ablation during the flame test, just after withdrawal of the flame and after ablation.

Char formation provides ablation- and flame-resistant properties to the composite, which were quantified by calculating its linear (LAR) and mass (MAR) ablation rates. The MAR and LAR of pristine RF samples were computed to be 0.079 mm s^{-1} and 0.050 g s^{-1}. The MAR was also computed for phenol formaldehyde to confirm the superiority of RF over PF under similar conditions and was found to be 0.087 g s^{-1}.[21,44] Rates reduced from 0.050 mm s^{-1} and 0.079 g s^{-1} for pristine RF to 0.019 mm s^{-1} and 0.053 g s^{-1} for 5 wt% CS/RF, respectively (Table 2). The reduction in LAR is accounted for by the presence of insulating carbon soot in the matrix, which impedes the spread of oxygen and further prevents combustion,[54,55] thereby slowing the extent of pyrolysis in the matrix and, as a result, reducing the LAR. The aromatic ring structures present in the composite, belonging to the matrix and the combusted hydrocarbon, can be termed physical heat sinks and are responsible for absorbing a major part of the heat supplied. Moreover, the amount of porous carbonaceous char increases as ablation progresses[56] and, as access of oxygen to the inner zones is limited, the amount of material exposed to the flame is reduced,

which hence causes a reduction in the MAR. However, as expected, the 10 wt% composite exhibited higher ablation rates, suggesting that the increased amount of CS in the matrix might have restricted the polymerization of RF during curing, thus forming a non-continuous polymer chain, resulting in composite highly vulnerable to erosive forces. Table 2 clearly shows the changes in weight and dimensions using various concentrations, and their effects on the respective ablation rates. The tables also point out the reduction in the ablation rates when compared to pristine RF. Modification of RF with camphor soot, in contrast to the addition of SiC, as determined by Badhe et al.,[19] has been found to lead to a marginal deterioration in terms of LAR and MAR, though the extremely low price of carbon soot, like boric acid in the case of another work by Badhe et al.,[36] makes it economically a more viable solution. Also, the reduction in the difference between the densities of the matrix and the filler is greater in the case of SiC and thus provides a better molecular-level dispersion.

Furthermore, the back-face temperature of the ablative composites was measured by a simple arrangement using a thermocouple and a ceramic insulator plate fixed at the test table, in accordance with ASTM E457-08 for measuring heat transfer rate. The delay in the temperature confirms that the insulation properties improved when increasing the filler content to evaluate the composites' thermal insulating properties during and after ablation. The energy and heat from the incoming flux during re-entry is consumed in ablation by the high bond dissociation energies of the aromatic rings in the polymeric matrix. This is an endothermic process which involves the absorption of a large amount of heat. Bond dissociation of the polymer chain of a phenolic polymer matrix is a highly endothermic process, by virtue of which the bonds break, absorbing a large amount of the incoming heat flux during re-entry conditions.[36] Consequently, the maximum back-face temperature (T_{max}) of all the polymer matrix composites ablated for 60 s was found to be below 150 °C. The rate of increase in the back-face temperature was found to be slightly higher than for pristine RF in the case of CS/RF composites, as well as a noticeable decrease observed in the temperature after withdrawal of the flame after 300 s. The decrease in the temperature profiles (Fig. 5) could be because of the increase in filler concentration and a consequent increase in the material's insulation properties with lower erosion, which provides protection from the flame more effectively.[44] Moreover, a shift was observed in the peak of the temperature profiles of the CS/RF composites, due to a slow increase in heat as the concentration of camphor soot increased, which confirms the improved insulation properties when increasing the filler loading.[57]
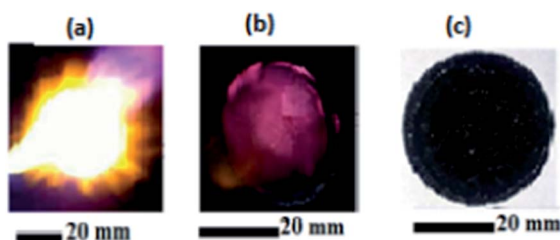
Theoretical surface ablation rates

Theoretical surface ablation rates were calculated by Lin[58] for quasi-steady ablation, assuming a unidirectional heat source for ablation under the influence of a steady heat source with constant flux. The energy balance of a heated surface for steady ablation can be given as eqn (1):
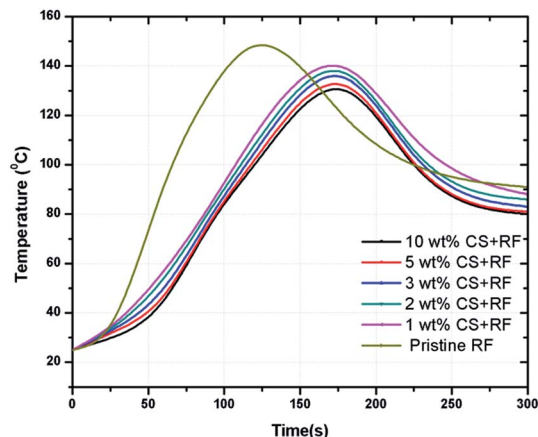

Fig. 4 Photographs of the specimen (a) during ablation (b) just after ablation (c) after ablation.

Fig. 5 Back-face temperature profile of the studied ablative composites.

$$q_{net} = \rho_w v_s \Delta H_{ab} - \left(k \frac{dt}{dy} \right) \bigg| y = 0 \qquad (1)$$

where ΔH_{ab} represents the net absorbed heat per unit loss of mass from the surface of the ablator, involving the effects of sublimation, evaporation, combustion, oxidation, or mechanical erosion, while q_{net} involves the effects of heating, re-radiative cooling, convective heating or cooling, or transpiration cooling. For a steady temperature gradient, we can consider $y = 0$ and, using the expression for a steady temperature gradient for the ablator, we get eqn (2), which denotes the theoretical solution of a steady ablation rate for a semi-infinite charring ablator.

$$v_s = \frac{q_{net}}{\rho_w \Delta H_{ab} + \rho_w H_w - \rho_v H_i + (\rho_v - \rho_w) H_{gw}} \qquad (2)$$

Considering that assumptions made by Lin[58] to obtain a detailed treatment and attain deeper physical insight of the ablation mechanism hold true, and assuming the presence of char, the steady ablation rate was expressed and is quoted from Lin as eqn (3):

$$v_s = \frac{q_{net}}{\rho_c \Delta H_{ab} + (\rho_v - \rho_c)\Delta H_0 + [\rho_c C_{pc} + (\rho_v - \rho_c)C_{pg}](t_w - t_0) - \rho_v C_{pv}(t_i - t_0)} \qquad (3)$$

The above-mentioned equation was solved for a theoretical ablation rate, using the parameters in Table 3. The parameters assumed here are applicable to the present oxyacetylene test specifications and others have been taken from a realistic range for a general case of a charring ablator. The results from these theoretical calculations give a general ablation rate for conventional ablators which have been widely used to date.[22,23]

This calculation gives a steady ablation rate of 0.083 g s⁻¹, which is in accordance with the ablation rates found for phenol

formaldehyde experimentally by us and by Srikanth *et al.*[22] of 0.087 mm s⁻¹. However, this rate is of a higher magnitude than the experimental ablation rates occurring in the present material. This observation gives an indication of the better ablation properties of RF/CS composites than conventional charring ablators.

Thermogravimetric analysis

Compared to other ablative composites,[21,44,59,60] CS/RF achieved a relatively high char yield (Table 2), which reached 59.7% after addition of 5 wt% CS to pristine RF, which exhibited a char yield of 45.8%. However, at 10 wt% loading of CS, there was no notable change in the percentage char yield, perhaps due to agglomeration of carbon nanomaterials leading to inadequate dispersion. Typical of the degradation of phenolic resins, the TGA graphs (Fig. 6) for all samples feature three thermal degradation zones. The first zone (100–300 °C) represents the removal of water and decomposition of free molecules and/or imperfectly crosslinked components,[61] while the weight loss in the 350–500 °C and 500–800 °C zones corresponds to decomposition of the polymer, which forms insulating carbonaceous char leading to the evolution of volatile gases. Pristine PF and RF exhibited a lower temperature for the first degradation step, at ≈300 °C. With the addition of camphor soot and an increase in its concentration, a gradual increase in the temperature of the first step of degradation occurred, from around 330 to 350 °C. This can be attributed to insertion of insulating carbonaceous filler in the matrix, which delays the spread of oxygen and the degradation front, resulting in an intumescent matrix. The second zone of degradation extended from 300–450 °C to 330–500 °C in the case of pristine PF, RF and carbon soot composites, respectively. Along with the increase in percentage char yield, it is seen that the use of resorcinol and addition of CS to RF improved the thermal stability of the composite. The third zone of degradation, which commences at ≈450 °C in the case of PF and RF, is seen to be delayed to 500 °C for camphor soot composites. This phenomenon, again, is attributed to absorption of the heat by insulating carbonaceous filler particles embedded in the three-dimensional matrix. These aromatic carbocyclics have been shown to form a high

percentage of intumescent char which includes tough carbonaceous residues that remain strongly bonded to the underlying material. Hence, as superior ablation rates and thermal stability were obtained for the CS/RF system, it provides a better cost-effective substitute for present ablative composites. Char consists of a carbonaceous porous turbostratic structure which assists in releasing pyrolysis gases, leading to a negative flux against the convective flux of heat, thereby increasing the thermal insulation. An increase in the concentration of

Table 3 Parameters for calculation of theoretical ablation rate for conventional ablator[58]

Parameter	Symbol	Value
Initial temperature	t_i	303 K
Net heat flux imposed upon the heated surface	q_{net}	0.5×10^6 W m^{-2}
Density of virgin ablator	ρ_v	~1200 kg m^{-3}
Specific heat of virgin ablator	C_{pv}	1800 J kg^{-1} K^{-1}
Density of char	ρ_c	800 kg m^{-3}
Specific heat of char	C_{pc}	2520 J kg^{-1} K^{-1}
Specific heat of pyrolysis gases	C_{pg}	1520 J kg^{-1} K^{-1}
Ablation temperature	t_{ab}	~2600 K
Effective ablation heat	ΔH_{ab}	0.7×10^6 J kg^{-1}
Pyrolysis heat at the reference temperature	ΔH_0	0.5×10^6 J kg^{-1}
Reference temperature at which the enthalpy of formation is defined	t_0	298 K

camphor soot had dramatic effects on the char residue of the composite up to 5 wt%, due to an increase in the amount of insulating char formed with an increase in the concentration of camphor soot. However, the thermograms do not show any marked rise in char yield beyond 5 wt%, for 10 wt% CS + RF composites, up to 800 °C. Since TGA characterization cannot reproduce any shear force caused by combustion gases, it is not possible to evaluate the effect of erosive forces on the charred composite.[57] Even so, as seen earlier, there is an increase in the MAR and LAR on incorporation of camphor soot beyond 5 wt%, where it was exposed to shearing and erosive forces. It was observed by Liu *et al.*[62] that carbon nanomaterials impair the thermal conductivity of polymer composites, which depends on their microstructure (cracks, chain spacing, porosity *etc.*) and lattice vibrations. Carbon soot loadings, thus, may have increased the chain spacing, resulting in lower thermal conductivity, which ensures a lower rate of heat transfer through the thickness, thereby maintaining the integrity of the polymer matrix for longer durations.

A carbonaceous char layer was formed after thermal degradation of the resin, the formation of which has long been recognized as an efficacious way of enhancing the fire retardancy of polymers.[63] Char formation, being an endothermic process, critically defines the heat dissipation properties of ablative composites. A char layer dissipates a large fraction of the incident convective heat flux through surface radiant emission.[22] Therefore, along with efficient char formation, char retention for an extended duration guarantees better thermal insulating properties during re-entry conditions (Fig. 7).

Composition and microstructure analysis

Microstructure studies revealed that the erosion and pyrolysis occurring upon ablation to CS/RF composites were substantially less than those of pristine RF. Also, a microstructure study of the composite's surface obtained after pyrolysis at 800 °C using a muffle furnace revealed the formation of a non-uniform pattern of insulating char (Fig. 8(a)). This insulating turbostratic carbon char was formed after ablation of RF resins, as indicated by the following reaction:[44,64]
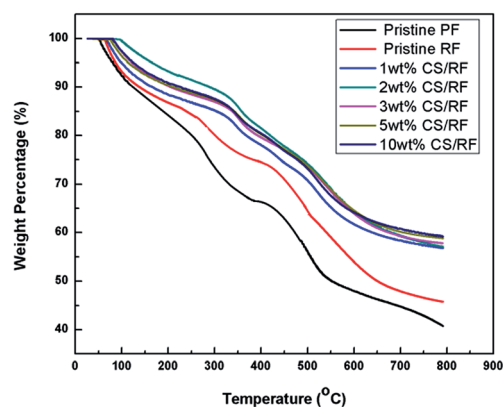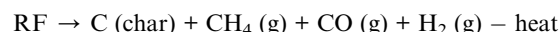
$$RF \rightarrow C \text{ (char)} + CH_4 \text{ (g)} + CO \text{ (g)} + H_2 \text{ (g)} - heat$$

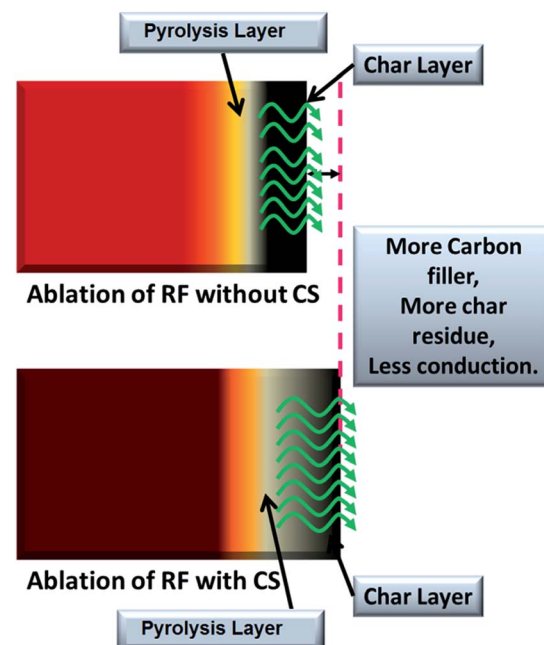**Fig. 6** TGA thermograms of the CS/RF composites at different concentrations.
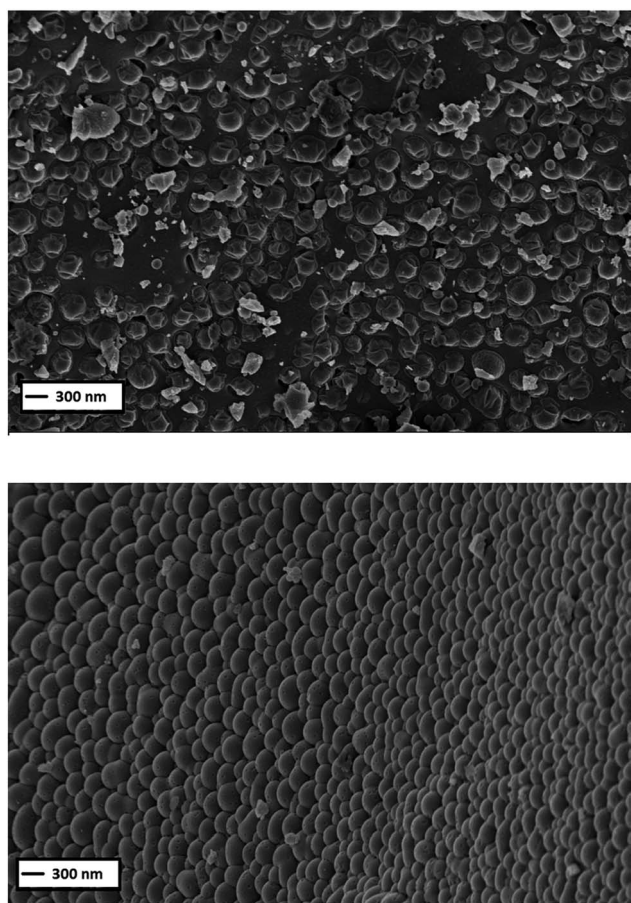

Fig. 7 Ablation scheme of RF without and with CS.

Fig. 8 Morphology of (a) surface ablated at 800 °C using muffle furnace, (b) surface ablated at around 3000 °C using oxyacetylene flame at 30k× magnification.

Fig. 9 Degradation mechanism of RF: type 1.

This degradation is found to occur *via* two mechanisms and is believed to follow degradation mechanisms similar to that of phenol. A typical degradation reaction of resorcinol formaldehyde is given in Fig. 9. In this reaction, the first step of thermo-oxidative degradation is the formation of a hydroperoxide structure, followed by decomposition to subsequent structures. According to Knop *et al.*,[65] the methylene bridges are the thermodynamically most stable crosslinking sites, while carbon dioxide and carbon monoxide are released as gaseous products. Moreover, another type of reaction has been proposed to take place during degradation, which involved the formation and evolution of methane gas as shown in Fig. 10. This type of fragmentation suggests hydrogen abstraction, driving the formation of a large amount of methane above 400 °C.[65,66] These reactions depict the proposed reaction mechanisms of the changes in the structure of the resorcinol formaldehyde matrix which lead to char formation and volatiles. The rigid three-dimensionally crosslinked structure resists thermal stress without softening or melting.[65] The decomposition and volatilization of flammable low-molecular-weight species are greatly favoured by these morphological characteristics. As RF is ignited or exposed to extremely high temperatures, it is transformed into a char-formi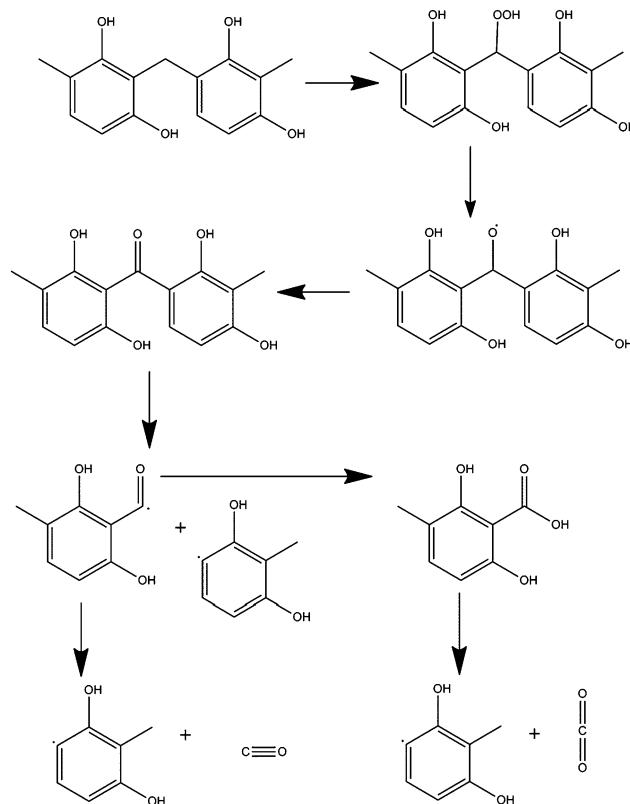ng material. The resorcinol structure facilitates the formation of a high carbon char that radiates heat and functions as an excellent heat insulator. The stability and concentration of the dihydroxyphenylmethane units formed from the methylene bridges affects the degradation process to a great extent. The first step of the thermo-oxidative degradation is the formation of a hydroperoxide, followed by decomposition to dihydroxybenzophenone and benzhydrol structures.[66] There is no change in the decomposition chemistry due to the addition of carbon soot particles, except for a delay and halt in the degradation process, due to the presence of insulating carbonaceous material as a filler in the vicinity of the polymer chains which delays the arrival of the heat flux and oxygen, thereby retarding decomposition, and a high char yield, giving rise to thermal resistance.[67,68] Therefore, it was speculated that the shielding action of the carbonaceous intumescent char against heat flux, due to its acting as a physical barrier against heat transmission to the underlying material, was aided by the
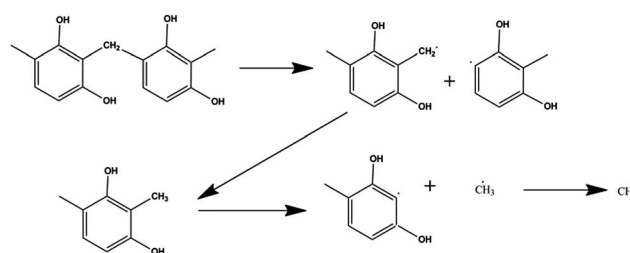

Fig. 10 Degradation mechanism of RF: type 2.

modifications of the chemical-physical structure of the intumescent char induced by the carbon nanoparticles.

There are numbers of pores, which result from pyrolysis of the phenolic resin matrix, pits and cracks in the char, which allow pyrolysis gases to flow out of the matrix, and from a gas flux moving outwards.[69–71] However, in some places, an oxygen molecule may penetrate deep inside the matrix and lead to a reaction, thus causing an acceleration in ablation by oxidation of the carbonized matrix. However, due to the presence of homogeneously dispersed carbon soot that forms a closely knit nanobead-like structure on the surface of the char, most of the pores are blocked. Hence, the arrival of oxygen and heat flux is restricted and thereby the thermal stability increases.

The surface ablated for 60 s using an oxyacetylene flame shows the presence of a closely knit carbon nanobead-like structure (Fig. 8(b)). The two FESEM images show the subsequent stepwise formation of the nanobead structure with an increase in temperature. The presence of turbostratic char was also confirmed by the peak at 24° (ref. 34) in the XRD spectra (Fig. 11), which also indicate an amorphous crystallographic structure with two broad maxima at 2θ angles of 24° and 44° corresponding to (002) and (100) planes, respectively, which reconfirms the existence of insulating turbostratic carbon,[72] regarded as a variant of h-graphite.[73] The diamond-like carbon particle structure is confirmed by the peak at 43° for the (111) plane, as also reported by Sahoo *et al.*[35] This peak seems to have merged with the (100) peak for charred carbon in the case of ablated RF + CS. The presence of this structure in unablated RF/CS is also prominent, attributed to the amorphous carbon system of the camphor soot, in contrast to the diffractogram of pristine RF. This structure provides high oxidation resistance coupled with configurational stability at extremely high temperatures, as compared to pristine RF, and assists control of heat transfer to the matrix.[19] Because of the formation of turbostratic carbon char at high temperatures, the amorphousness of the system increases, resulting in broad peaks. Turbostratic carbon is known to be a highly disordered carbon structure, similar to graphite, in which structural units consisting of hexagonal planes of carbon are bonded to each other by sp²

bonds.[19] The flame retardancy of the modified resin is enhanced, due to its intumescent properties and the formation of insulating carbonaceous char which consumes and removes oxygen, thereby preventing advance of the charred layer further into the matrix. A decrease in the repulsive interaction between the p-electron clouds of adjacent layers, causing them to come together, results in a minute increase in the crystallinity of the otherwise amorphous carbon.[72] The following proposed ablation mechanism explains the microstructure and composition thus formed, which provide the enhanced char retention and ablation resistance of the CS/RF nanocomposite.

Fig. 12(a) and (b) show 3-D atomic force microscopy images of the surface of the sample, clearly indicating a nanospike-like morphology which proves to be beneficial for penetrating the atmosphere. This causes minimal damage to itself and thereby is extremely capable of tolerating the impact of collision and producing consequent shock waves.[74] Fig. 12(a) presents the 3D representation of the ablated RF whereas Fig. 12(b) refers to the ablated CS/RF composite, where pristine RF shows a rougher morphology than ablated CS/RF. It is evident from various literatures that a surface having more roughness is more prone to mechanical erosion, as this tends to increase surface reactivity, promoting turbulent transitions in the heat flow which cause a rise in surface erosion.[75–78] Hence, it can be concluded that the addition of carbon soot to the polymeric matrix results in a decrease in mechanical erosion.

Contact angle measurement

The interaction between the surface of the composite and water molecules was analysed for the measurement of its water contact angle, to determine its hydrophilic or hydrophobic property. The water contact angle on a slide of the composite depends upon the surface energy between liquid, solid and vapour states.[14,79] It was assumed that the orientation of the
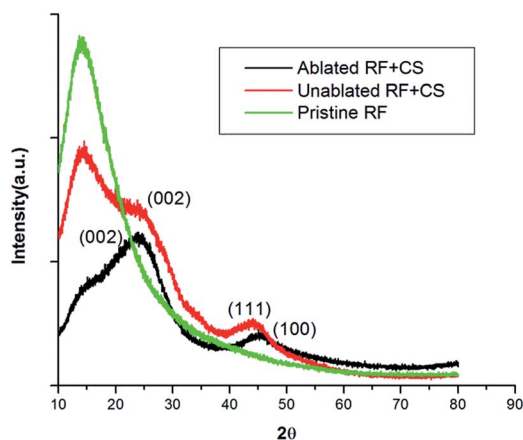
Fig. 11 X-ray diffraction pattern of ablated and unablated CS/RF and pristine RF depicting planes for turbostratic carbon.
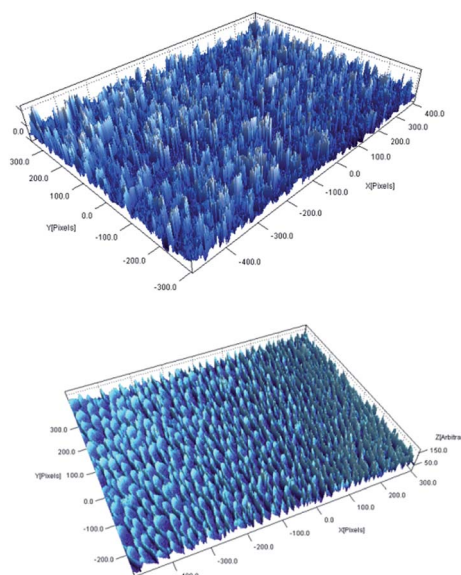
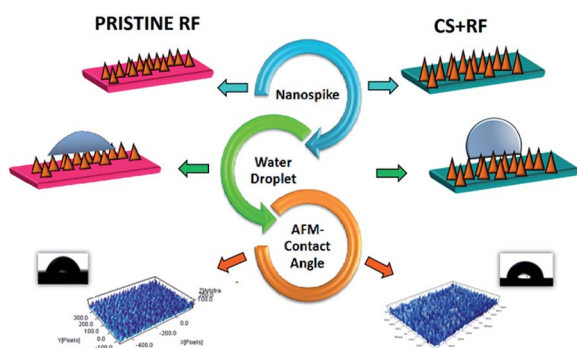**Fig. 12** AFM topographies of (a) ablated pristine RF (b) ablated CS/RF.

Table 4 Contact angle measurements of composites

Composition	Contact angle	
Pure RF	81.2	
1% CS + RF	83.3	
2% CS + RF	85.1	
3% CS + RF	89.7	
5% CS + RF	93.4	
10% CS + RF	101.8	

filler units, which have lower density as compared to the polymer resin, in the relevant nanostructure was preferably on the air side, a position which creates a protective layer over the polar groups of the polymer.[58,80,81] We anticipated that the carbon soot in CS/RF nanocomposites was also oriented towards the air side to form a protective layer on the surface of the polymer matrix composite. To prove this result, the contact angles of heat-treated PF, RF and CS/RF were measured (Table 4) and, as the percentage loading was increased, the contact angle also increased. This increase in hydrophobicity was attributed to enrichment of the polymer surface with CS, which alone exhibits superhydrophobicity,[35] indicating a lower surface energy because of a relatively small number of polar groups present on the surface. Adding to the effectiveness of CS/RF nanocomposites, they achieved a higher contact angle value for the same concentration of CS units in polymer resins under similar conditions. It increased from 81.2° for neat RF to 101.8° for 10 wt% CS/RF. Fig. 13 shows a schematic of the correlation of the surface properties of the composites with the water contact angle. This indicates that the inclusion of carbon nanomaterials created a shield of carbon soot on the surface polar group, which gave rise to an even more enhanced surface barrier property.[37,82]

Ablation mechanism

A porous carbonaceous zone is seen to be formed by pyrolytic degradation of the matrix resin with the advance of the pyrolytic front into the virgin material, as seen in Fig. 14, depicting the erosion mechanism of a charring ablator. The substructure can be seen on the left, extending to the ablating surface. During the pyrolysis process, the pyrolyzing phase of the material, which is the outermost layer, in contact with the outer environment, carbonizes, loses mass, producing pyrolysis gases, and advances into the material. A boundary layer of low pressure is created due to the advent of hypersonic hot air above the ablation surface. Heat is circulated and dissipated from the boundary layer away from the surface, leading to potent heat shielding.[83] The pore network of the turbostratic char, with micro-cracks, allows gaseous decomposition products, such as hydrogen, ammonia and hydrocarbons, to pass through *via* diffusion. These gases are ejected at elevated velocities, undergoing heat exchange with the surroundings, and escape from the surface at the boundary layer. This departure of gases retards the convective flux approaching the material by interfering with the flow field.[65]

During the oxyacetylene flame test, in the case of plain RF, as a critical amount of char was formed, the remnant RF resin was unable to hold the char layer together against the prevailing oxyacetylene flame's erosive conditions, leading to higher ablation rates. However, in the case of CS-infiltrated RF composites, when the temperature goes beyond 1000 °C, pyrolysis of the additive takes place and results in the formation of highly reactive open-book-like structures of hexagons, pentagons or both rings together,[33] which act as the basic building blocks required to form spherically shaped carbon nanobeads.[34] These reactive rings may have reacted with the carbon char forming a closely knit carbon nanobead-like structure (Fig. 7(b)). Hence, the underlying polymer matrix and the char formed from it were held together firmly, improving the char retention property. This ensures complete

Fig. 13 Schematic of variation in contact angle depending upon nanospike height.
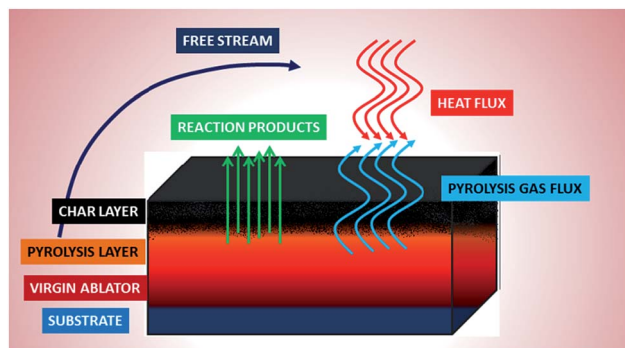
Fig. 14 Zones of ablation formed during pyrolysis of a charring ablator.

charring of the resin, thereby dissipating more heat and reducing erosive losses during ablation. Furthermore, the insulating char restricts the advance of heat, improving the ablation resistance. Thus the formation of a carbon nanobead-like structure acts on the surface, resisting an oxyacetylene flame and ensuring enhanced ablation resistance. However, carbon char formation operates beneath the exposed surface, providing enhanced insulating properties to the composite. However, in the case of 10 wt% CS/RF, the outgoing gases produced during thermal decomposition of RF may have found it difficult to escape through the surface, which led to pressure building up inside the surface of the ablating specimen, leading to lifting of the surface or partially collapsed bubbles. This exposed the internal surface of 10 wt% CS/RF to the flame, thereby leading to pyrolysis of the underlying zone at a faster rate, increasing its ablation rate.

Conclusion

The phenomenon of ablation using tailored thermoset composites has been pursued using a novel approach, which takes into account the enhancement of properties as compared to conventional composites. The synthesis of an ablative composite of resorcinol formaldehyde modified with carbon soot has been successfully proposed for such applications and studied thoroughly with respect to its thermal aspects. Furthermore, upon comparison of the density, contact angle values and ablation rates of PF and RF, measured in similar circumstances, it is conceivable that RF could be effectively used instead of PF as a polymer resin. CS/RF composites attained a relatively higher char yield, up to 59.7% at 800 °C, and exhibited excellent ablation resistance, with a linear ablation rate of 0.019 mm s^{-1} and a mass loss rate of 0.053 g s^{-1}. The enhanced ablation resistance was attributed to the formation of insulating turbostratic carbon char and a closely knit carbon nanobead-like structure, which impedes ablation by acting as an excellent barrier for blocking the passage of oxygen. Hence, carbon soot-doped resorcinol formaldehyde ablative composites open up the possibility to formulate relatively thinner ablative PMC to reduce the overall weight of the TPS used in aerospace vehicles. Controlled and optimized quantities of suitable filler like camphor soot can offer significant ablation resistance for the extreme hyperthermal conditions during re-entry, along with reduced thermal decomposition, to provide significant weight savings for aerospace systems.

Acknowledgements

References

1 R. Yadav, G. Velidi and U. Guven, Aerothermodynamics of generic re-entry vehicle with a series of aerospikes at nose, *Acta Astronaut.*, 2014, **96**, 1–10, DOI: 10.1016/j.actaastro.2013.11.015.

2 R. A. Vaia, G. Price, P. N. Ruth, H. T. Nguyen and J. Lichtenhan, Polymer/layered silicate nanocomposites as high performance ablative materials, *Appl. Clay Sci.*, 1999, **15**(no. 1–2), 67–92.

3 M. Aldridge, A. Waas and J. Kieffer, *Compos. Sci. Technol.*, 2014, **98**, 22.

4 D. W. K. Ho, J. H. Koo and O. A. Ezekoye, *J. Spacecr. Rockets*, 2009, **46**, 526.

5 G. Pulci, J. Tirillò, F. Marra and F. Fossati, *et al.*, *Composites, Part A*, 2010, **41**, 1483.

6 M. O. Abdalla, A. Ludwick and T. Mitchell, *Polymer*, 2003, **44**(24), 7353.

7 A. M. Kawamoto, L. C. Pardini, M. F. Diniz, V. L. Lourenco and M. F. K. Takahashi, *J. Aerosp. Technol. Manage.*, 2010, **2**(2), 169.

8 H. Yu, J. Liu, X. Wen, Z. Jiang, Y. Wang, L. Wang and J. Zheng, *Polymer*, 2011, **52**(21), 4891.

9 Y. Zhang, S. Shen and Y. Liu, *Polym. Degrad. Stab.*, 2013, **98**(2), 514.

10 D. Cho, Phenolic, *J. Mater. Sci. Lett.*, 1996, **15**, 1786.

11 T. L. Dhami, O. P. Bahl and B. R. Awasthy, *Carbon*, 1995, **33**(4), 479.

12 S. Kuo, C. Huang and F. Chang, *Macromol. Rapid Commun.*, 2006, 537–541.

13 P. Xu and X. Jing, *Polym. Eng. Sci.*, 2010, **50**(7), 1382.

14 J. Xiao, J.-M. Chen, H.-D. Zhou and Q. Zhang, *J. Mater. Sci. Eng. A*, 2007, **452–453**, 23–30.

15 R. D. Patton and C. U. Pittman, *Composites, Part A*, 2002, **33**, 243–251.

16 J. H. Koo and L. A. Pilato, *41st AIAA–ASME–SAE–ASEE, Joint Propulsion Conference & Exhibit*, Tucson, AZ, 2005.

17 J. K. Park, D. Cho and T. J. Kang, *Carbon*, 2004, **42**, 795.

18 J. T. Mottram and R. Taylor, *Compos. Sci. Technol.*, 1987, **29**, 189.

19 Y. Badhe and B. Kandasubramanian, *RSC Adv.*, 2014, **4**, 28956.

20 R. Durairaj, *Resorcinol, Chemistry, Technology and Applications*, Springer-Verlag, Berlin, Heidelberg, Germany, 2005, pp. 180–182.

21 K. Balasubramanian and Y. Badhe, Cost Effective Processing Of Defect/Blister Free Ablative Composites Of Functionally Tailored Resins Of Ultra High Temperature Ceramics For Layered Composite, Indian Patent, 641/MUM/2014, 2014.

22 I. Srikanth, A. Daniel, S. Kumar, N. Padmavathi, V. Singh, P. Ghosal, A. Kumar and G. Rohinidevi, Nano silica modified carbon–phenolic composites for enhanced ablation resistance, *Scr. Mater.*, 2010, **63**, 200–203.

23 R. P. Nathan and S. Bindu, in *Low Temperature Ablative Heat Shield for Re-Entry Vehicles, Proceedings of AIAA Thermophysics Conference*, Ontario, Toronto, Canada, 2005.

24 S. J. Delmonte, *The Tech. Of Adhesives*, Reinhold, 1947, ch. 2, p. 26.

25 A. Pizzi, *Handbook of Adhesives technology*, Ecole Nationale Supérieure des Technologies et Industries du Bois, Université de Nancy I, Epinal, France, ch. 29, 2003.

26 H. E. Euler, *Angew. Chem.*, 1941, **54**, 458.

27 J. A. Brydson, *Plastic materials*, Butterworth Heinemann, 7th edn, 1999, p. 645.

28 Q. Zhou, Z. Zhao, Y. Zhang, B. Meng, A. Zhou and J. Qiu, *Energy Fuels*, 2012, **26**, 5186.

29 B. Q. Wei, R. Vajtai, Y. Jung, J. Ward, R. Zhang and G. Ramanath, *Nature*, 2002, **416**, 495.

30 S. Cui, C. Z. Lu, Y. L. Quio and L. Cui, *Carbon*, 1999, **37**, 2070.

31 K. Mukhopadhyay, I. Mukhopadhyay, M. Sharon and T. Soga, *Carbon*, 1997, **35**, 863.

32 K. Mukhopadhyay, K. M. Krishna and M. Sharon, *Mater. Chem. Phys.*, 1997, **49**, 252.

33 K. Mukhopadhyay, K. M. Krishna and M. Sharon, *Carbon*, 1996, **34**, 251.

34 M. Sharon, K. Mukhopadhyay, K. Yase, S. Iijima and Y. Ando, *Carbon*, 1998, **36**, 507.

35 B. N. Sahoo and B. Kandasubramanian, *RSC Adv.*, 2014, **4**, 11331.

36 Y. Badhe and K. Balasubramanian, *RSC Adv.*, 2014, **4**(82), 43708–43719.

37 B. N. Sahoo and K. Balasubramanian, *J. Colloid Interface Sci.*, 2014, **436**, 111–121.

38 P. Mishra and K. Balasubramanian, *RSC Adv.*, 2014, **4**, 53291–53296.

39 N. Singh and K. Balasubramanian, *RSC Adv.*, 2014, **4**, 27691–27701.

40 M. Natali, M. Monti, D. Puglia, J. M. Kenny and L. Torre, *Composites, Part A*, Jan. 2012, **43**(no. 1), 174–182.

41 C. Hong, J. Han, X. Zhang and H. David, *et al.*, *Composites, Part Bs*, 2012, **43**, 2389.

42 Y. Zeng, X. Xiong, G. Li, Z. Chen, W. Sun and D. Wang, *Carbon*, Apr. 2013, **54**, 300–309.

43 X. Yao, H. Li, Y. Zhang, K. Li, Q. Fu and H. Peng, *J. Therm. Spray Technol.*, Mar. 2013, **22**(no. 4), 531–537.

44 I. Srikanth, N. Padmavathi, S. Kumar and A. Kumar, *et al.*, *Compos. Sci. Technol.*, 2013, **80**, 1.

45 D. Zhao, C. Zhang, H. Hu and Y. Zhang, *Compos. Sci. Technol.*, Jul. 2011, **71**(no. 11), 1392–1396.

46 Y. Zhu, S. Wang, W. Li, S. Zhang and Z. Chen, *Scr. Mater.*, 2012, **67**, 822.

47 B. P. Wilson, Ultrasound, Cavitation and Cleaning, B.Sc. Hon's (Wales) Thesis, Department of Materials Engineering University of Wales, Swansea, September 1997.

48 H. M. Santos, C. Lodeiro and J. e.-L. Capelo-MartRnez, *Ultrasound in Chemistry: Analytical Applications*, ed. J.-L. Capelo-Martínez, Copyright_, WILEY-VCH Verlag GmbH & Co. KGaA, Weinhein, 2009.

49 T. J. Mason and J. P. Lorimer, *Sonochemistry: Theory, Applications and uses of Ultrasound in Chemistry*, Wiley-Interscience, New York, 1989.

50 T. J. Mason, *Practical Sonochemistry: Users Guide to Applications in Chemistry and Chemical Engineering*, Ellis Horwood Ltd, New York, 1992.

51 T. J. Mason, *Sonochemistry*, Oxford Chemistry Primers, Oxford, UK, 2000.

52 T. J. Mason, J. P. Lorimer, F. Cuesta and L. Paniwnyk, *Ultrasonic International, Conference Proceedings*, 1989, p. 1253.

53 N. Iqbal, S. Sagar, M. B. Khan and H. M. Rafique, *J. Compos. Mater.*, 2013, **48**, 1221.

54 F. Laoutid, L. Bonnaud, M. Alexandre, J. Lopez-cuesta and P. Dubois, *Mater. Sci. Eng., R*, 2009, **63**, 100–125, DOI: 10.1016/j.mser.2008.09.002.

55 Z. Xinghong, H. Ping, H. Jiecai and M. Songhe, *Compos. Sci. Technol.*, 2008, **68**, 1718.

56 T. Shinn-Shyong and C. Ya-Ga, *Mater. Chem. Phys.*, 2002, **73**, 162.

57 M. Natali, M. Monti, J. M. Kenny and L. Torre, *Composites, Part A*, 2011, **42**, 1197.

58 W.-S. Lin, *Int. J. Heat Mass Transfer*, 2007, **50**(5–6), 1196–1201.

59 H. C. Lin, S. W. Kuo, C. F. Huang and F. C. Chang, *Macromol. Rapid Commun.*, 2006, **27**, 537.

60 Y. Jiang, X. Zhang, J. He, L. Yu and R. Yang, *Polym. Degrad. Stab.*, 2011, **96**, 949.

61 A. Trick and T. E. Saliba, *Carbon*, 1995, **33**, 1509.

62 H. Liu, S. Zheng and K. Nie, *Macromolecules*, 2005, **38**, 5088.

63 A. R. Bahramian, M. Kokabi, M. Hossein and N. Famili, *J. Polym.*, 2006, **47**, 3661.

64 R. A. Jones and G. M. Jenkins, *Carbon*, 1976, **76**, 27.

65 A. Knop and A. Louis, Pilato Applications and Performance Future Directions Modified and Thermal-Resistant Resins, *Phenolic Resins Chemistry*, 1985, pp. 147–155.

66 R. T. Conley, *Thermal Stability of Polymers*, Marcel Dekker Inc., New York, 1970, ch. 2.

67 N. B. Sunshine, Flame Retardancy of Phenolic Resins and Urea- and Melamine-Formaldehyde Resins, in *Flame Retardancy of Polymerie Materials*, Marcel Dekker, New York, 1973, vol. 2, ch. 4.

68 Y. Zaks, J. Lo, D. Raucher and E. M. Pearce, *J. Appl. Polym. Sci.*, 1982, **27**, 930.

69 Y. Chen, P. Chen, C. Hong, B. Zhang and D. Hui, Improved ablation resistance of carbon–phenolic composites by introducing zirconium diboride particles, *Composites, Part B*, Apr. 2013, **47**, 320–325.

70 R. A. Vaia, G. Price, P. N. Ruth, H. T. Nguyen and J. Lichtenhan, Polymer/layered silicate nanocomposites as high performance ablative materials, *Appl. Clay Sci.*, 1999, **15**, 67–92.

71 G. Gautherot, *Contribution a 'Hude de Ia degradationdes resines phenoliques*, Office national d'etudes et de recherches aerospatiales, 1969.

72 Y. Lui and X. Jing, *Carbon*, 2007, **45**, 1965.

73 F. Ji, Y. L. Li, J. M. Feng, D. Su, Y. Y. Wen and Y. Feng, *J. Mater. Chem.*, 2009, **19**, 9063.

74 W. Shepeard, Rocket Construction, US Patent, US 3001473A, 1961.

75 M. D. Jackson, *Interim report SAMSOTR7486 of Passive Nosetip Technology (PANT) Program No. 15*, 1974.

76 D. C. Reda, *Correlation of nosetip boundary-layer transition data measured in ballistic-range experiments*, Sandia Report SAND, 1979, vol. 790649.

77 R. G. Batt and H. H. Legner, A review of roughness-induced nosetip transition, *AIAA Pap.*, 1983, **21**, 7–22.

78 V. Borie, Y. Maisonneuve, D. Lambert and G. Lengellé, Ablation des matériaux de tuyères de propulseurs à propergol solide, Technical Report No. 13 ONERA, France, 1990.

79 B. N. Sahoo, B. Kandasubramanian and B. Sabarish, *eXPRESS Polym. Lett.*, 2013, **7**, 900.

80 S. Turri and M. Levi, *Macromolecules*, 2005, **38**, 5569.

81 S. Turri and M. Levi, *Macromol. Rapid Commun.*, 2005, **26**, 1233.

82 B. N. Sahoo and K. Balasubramanian, Recent progress in fabrication and characterization of hierarchical biomimetic superhydrophobic structures, *RSC Adv.*, 2014, **4**, 22053–22093.

83 C. Luo and P. E. DesJardin, *Compos. Sci. Technol.*, 2007, **67**, 1475.